ACADEMIA ROMÂNĂ
Revue Roumaine de Chimie
https://www.icf.ro/rrch/

Rev. Roum. Chim.,
2024, *69*(10–12), 565–571
DOI: 10.33224/rrch.2024.69.10-12.05

ZR-PILLARED MONTMORILLONITE CLAY AS HOST TO IONIC LIQUIDS FROM AQUEOUS SOLUTIONS

Abdeldjabbar BELBEL,*[a] Ahmed DRAOUI[a,b] and Kadour CHERAIF[a]

[a]Department of Physics, Ecole Normale Supérieure of Laghouat, 03000 Laghouat, Algeria
[b]Laboratoire de Physique des Matériaux (LPM), Université Amar Telidji de Laghouat, BP 37G, Laghouat 03000, Algeria
[b]Materials Physics Laboratory (LPM), Amar Telidji University of Laghouat, BP 37G, Laghouat 03000, Algeria

Received February 3, 2024

Zirconium-pillared montmorillonite was prepared in this work. Many methods, such as dynamic light scattering (DLS), thermogravimetric analysis (TGA), differential thermal analysis (DTA), and zeta potential (ζ) techniques, have been used to characterize clays and study particle size distribution and thermal behaviour. In addition, experimental conditions, including pH were evaluated. The montmorillonite powder was found to have a narrow particle size distribution with a peak at 147 nm, in addition, the pillared montmorillonite was negatively charged even at pH 3, and the strong negative surface charge of montmorillonite indicated that this clay can effectively remove organic molecule in water. The FT-IR analysis revealed that the pillaring with Zr did not destroy the initial structure of the sodium bentonite, and some characteristic bands of the intercalating agents appear. To obtain information on thermal stability and degradation products, the thermal properties of inorganics were investigated. These thermal measurements indicate that they inorganically display two distinct regions: (I) from RT to 173 ^{0}C corresponding to physical adsorption and removal of water of hydration, (II) dihydroxylation of the silicate structure in the temperature range of 300–800 ^{0}C. Adsorption isotherms displayed that the maximum adsorption capacity of Mt-Na and PMt-Na, according to the Langmuir model, were 54.77 mg/g and 22.70 mg/g, respectively.

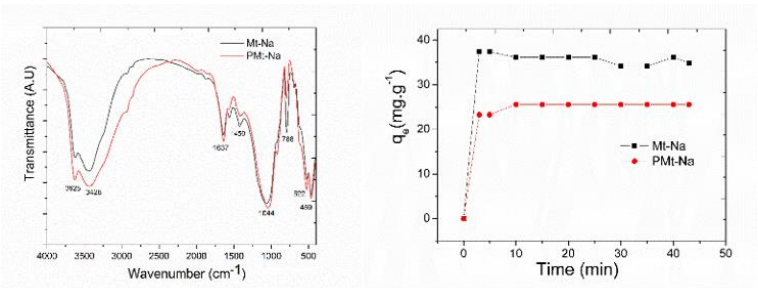

INTRODUCTION

Pillar clays are an entirely new family of interlayer clays. They are based on two-dimensional materials with a porous texture and a structure capable of being used in adsorption,[1] as well as in catalysis.[2] Ion exchange of the cations in the interlayer region of the clay by inorganic polyoxycations is typically used in their preparation. Heat converts these polyoxycations to the corresponding oxides, which act as props between the silicate layers, resulting in a microporous material with potential applications as a molecular sieve.[3,4] One of the most commonly used cations for pillaring up to the present is a polynuclear hydroxy zirconium complex with the structure shown below. $[Zr_4(OH)_{14}(H_2O)_{10}]^{2+}$.[5–7] Montmorillonite is a smectite clay mineral with a single octahedral layer between two silicon-oxide tetrahedral layers. Particle size is small, 0.01–1 m, with a high specific surface area 700–800 m^2/g, and a CEC of 80–100 meq/100 g.[8,9] Montmorillonite is used not only as a raw clay but also as an organo-clay, in which inorganic cations are

* Corresponding author: belbel.dj@gmail.com

exchanged for organic ones to modify surface area.[10] Adsorption of organic cations reduces the surface charge (makes it less negative) and, in many cases, results in charge reversal. As a result, cation adsorption can be monitored by measuring the change in zeta potential (ξ), of the clay surface, a relatively simple, quick, and inexpensive measurement that also provides information on the organo-clays' stability in dispersion.[11,12] Indeed (ξ), the potential between the slipping plane and the bulk solution, is an important electrokinetic property of clay minerals, which has traditionally been applied to measure the stability of clay dispersions,[13,14] as well as to describe clay aggregation, flow, sedimentation, and filtration.[15,16] (ξ) measurements, in addition to indicating colloid stability, are important in understanding the adsorption mechanism of inorganic and organic molecules at the solid/solution interface. The determination of montmorillonite clay surface properties is an important criterion for establishing its adsorption ability against anionic and cationic species from wastewater. In this study, the electrokinetic surface properties of montmorillonite were investigated using the microelectrophoresis technique.

EXPERIMENTAL

Materials and methods

SWy-2 montmorillonite from Crook County (Wyoming) was purchased at the Source Clays Repository (Clay Mineral Society ref: Srce Clay SWy-2, for more information, see http://www.clays.org/) and used without further purification. This clay mineral has the chemical formula.[17] [$Si_{7.89}$ $Al_{3.34}$ $Fe_{0.42}Mg_{0.56}$ $Ca_{0.52}$ $Na_{0.14}$ $K_{0.01}$]. Its cation exchange capacity (CEC) is reported to be about 75 meq/100g.[18]

Following the same procedure described previously, homoionic clay was prepared by exchanging ions between Mt and NaCl.[19] All of the chemicals used in this study, such as NaCl, $ZrOCl_2 \cdot 8H_2O$, HCl, and NaOH, were analytical reagent grade and obtained from the Guangzhou chemical reagent factory (Guangdong Province, China). The Butyl methylimidazolium chloride (BMIMCl), which were obtained from the Tokyo Chemical Industry (Japan). Zr-pillared montmorillonite was prepared by the following method: Adopted from Yamanaka and Brindley,[5] with slight modifications: appropriate volumes of $ZrOCl_2$, $8H_2O$ (0.1 M) were added to 3 g of Mt-Na and continuously stirred for 2 h at room temperature. Afterward, the clay suspensions were dialyzed against distilled water until chloride-free. Finally, the centrifuged solid, drying, is referred to as PMt-Na.

BMIMCl adsorption on material

The BMIMCl was adsorbed on the materials as follows: 50 mg of clays Mt-Na or PMt-Na was dispersed in 10 ml (or 30 ml) of water with BMIMCl concentrations from 0.5 to 4 $mmol \cdot L^{-1}$ for the isotherm study or 0.5 $mmol \cdot L^{-1}$ for the kinetic study. The mixture was stirred for 20 min at room temperature. For the kinetic study, the contact time was from 3 to 45 min by 5 min step. The supernatant was removed to measure the $BMIM^+$ concentrations by absorbance at the wavelength of 211 nm, corresponding to the maximum using a spectrophotometer (UviLine9400-SECOMAM).

Characterization

The particle size (diameter) in the 1–900 nm range was monitored using dynamic light scattering (Zetasizer Nano, ZS, HORIBA). Before testing, a clay suspension in distilled water was prepared, sonicated, and stored for 24 hours. To determine the points of zero charge, the zeta potential values of prepared material suspensions ($1.5g \cdot L^{-1}$) at different pH values were obtained. The clay samples ($1.5g \cdot L^{-1}$) were allowed to settle for approximately 1 h, and a few milliliters from the top of the dispersion was measured. Infrared (I.R) spectra were collected using a *Shimadzu Fourier Transform spectrometer* with a resolution of 2 cm^{-1} over a range of 400 to 4000 cm^{-1}, approximately 0.5 mg clay were finely grounded and mixed with KBr. This mixture was pressed pressure in a die to produce a pellet. In order to evaluate the thermal stability of the homoionic clay and modified it, thermo-gravimetric analysis (TGA) and differential thermal analyses (DTA) were performed with a (LABSYS evo) instrument using 40 mg samples. In a nitrogen atmosphere, the samples were heated at a rate of 5 °C/min from room temperature to 1000 °C.

RESULTS AND DISCUSSION

Dynamic light scattering (DLS)

The DLS results for the Mt particle size distribution are shown in Fig. 1a As shown, the sizes of most of the particles lie within the range from

1 to 900 nm. The particle size distribution is monomodal, with a peak at 147 nm.

The concentration of solids in solution is a major determinant of surface charge generation. To investigate the effect of solid-to-solution ratio on zeta potential, different montmorillonite dispersions were prepared in distilled water at concentrations ranging from 0.05 to 0.3 ($g \cdot L^{-1}$), and their zeta potentials were measured Fig. 1b. It was found that clay samples ($1.5 g \cdot L^{-1}$) had an average zeta potential of –96.6 mV. As a result, subsequent experiments were carried out at a solid-to-solution ratio of 1.5 $g \cdot L^{-1}$.[20]

The zeta potentials of PMt and Mt in aqueous solutions with varying pH values are depicted in Fig 2. Mt-Na has constant negative values throughout the pH range, indicating a highly negatively charged surface. The pillaring step places a prominent influence on the surface property of Na-Mt. Clearfield,[21] proposed that tetrameric $[Zr(OH)_2 \cdot 4H_2O]_4)^{8+}$ cations present in the solid phase of zirconium oxychloride hydrolyze when dissolved in water to yield deprotonated species with reduced charge. Even at pH 2.7, montmorillonite particles did not have a point of zero charge.

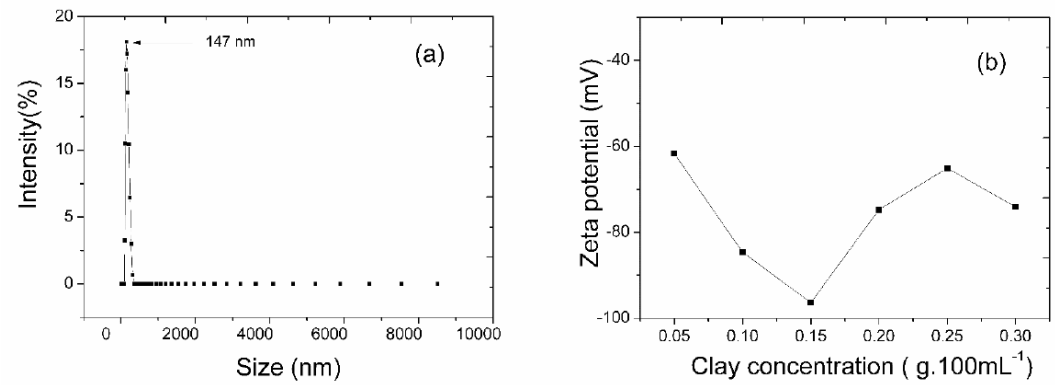

Fig. 1 – Characterization of Mt: a) DLS particle-size distribution; b) Zeta potential as a function of solid concentration.

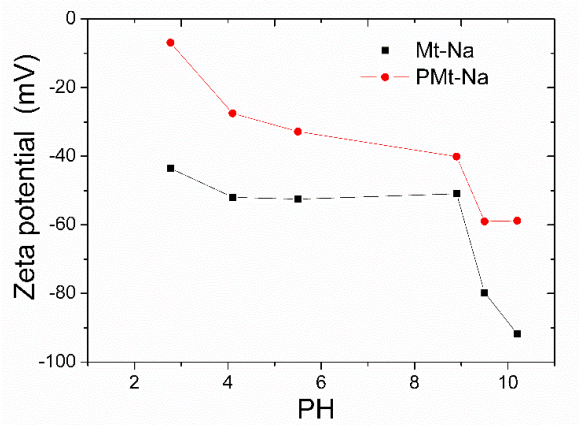

Fig. 2 – Zeta potential values as a function of pH ($1.5 g \cdot L^{-1}$ clay suspensions).

Thermo gravimetric analysis (TGA, DTA)

The thermal curves in the RT – 1000 ^{0}C range, corresponding to the starting Mt-Na and Zr-pillared clay at room temperature, are shown in Fig. 3. The general feature of the thermal curves reveals two steps: one, in the RT – 200 ^{0}C and the other in the 200–800 ^{0}C temperature ranges. The first step in Mt-Na has been attributed to physiosorbed and hydrating water, whereas the second is due to dihydroxylation of the silicate structure, which sometimes occurs dissociated in two, hardly visible here but clearly shown in the corresponding DTG Fig. 4 and, more importantly, in the ATD curves (in 586 ^{0}C and 660 ^{0}C) Fig. 5, denoting silicate structure dihydroxylation in two different environments, here Al and Mg, as a result of an important isomorphic substitution in the clay net with different bonding strengths between the Mt and the surrounding oxygen (or hydroxyl) ions.[22] Table 1 displays the losses associated with each region of Mt-Na and PMt. Because of the presence of hydroxy-Zr species and hydroxyl groups involved in water-water hydrogen bonds, the first loss is high in a sample PMt.[23] In good agreement with the FTIR data.

At low temperatures, the (DTA) plot corresponding to Mt-Na shows an endothermic peak. It is commonly thought to be caused by the loss of weakly bonded, physiosorbed water adsorbed on the clay's external surface, as well as interlamellar water coordinated to the exchangeable cations, in this case Na^+. A shoulder visible at around 466 ^{0}C arises because of the interlamellar water loss. The following two peaks result from dihydroxylation of the clay octahedral layer in different environments, at 586 ^{0}C from Al substituting Mg (or Fe) and at 666 ^{0}C from Al substituting Fe.[22] Both these endothermic peaks correspond to the losses detected by TGA in the same interval. Finally, an endothermic peak at around 890 ^{0}C is due to the final dihydroxylation and crystalline net destruction.

The DTA curve for the PMt Fig. 5 does not depart so much from the parent material, however, one additional characteristic of the curve is the loss of definition of the peaks at around 466 ^{0}C and 666 ^{0}C, visible in case of Mt-Na. These peaks in the parent clay were attributed to dihydroxylation from different environments, and interlamellar water loss.

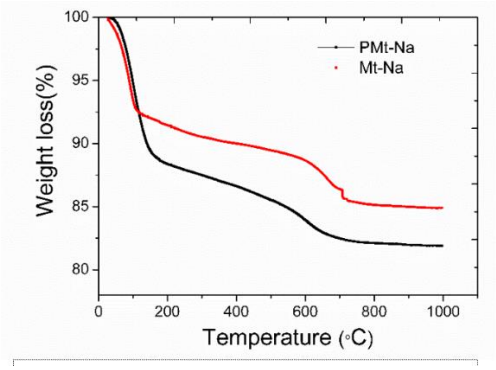

Fig. 3 – TGA curves of the Mt and PMt.

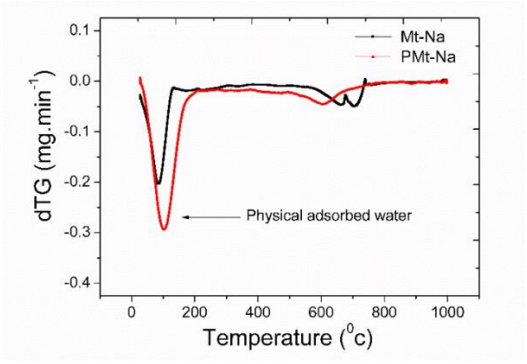

Fig. 4 –DTG curves of the Mt and PMt.

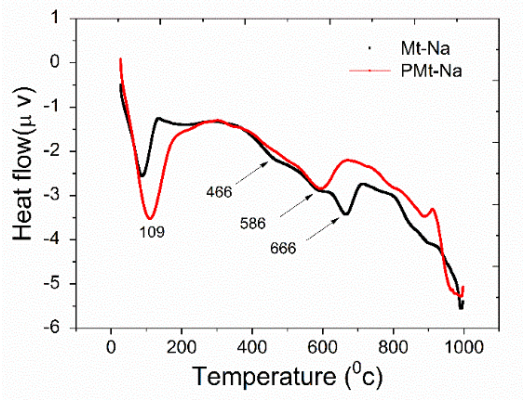

Fig. 5 – DTA curves of the Mt and PMt.

Table 1

Percent losses of the samples

Sample	25 (RT) –200 ^{0}C	200–800 ^{0}C	Total
Mt-Na	8.56 %	6.32 %	14.88 %
PMt-Na	11.58 %	6.34 %	17.92 %

FTIR analysis

Figure 6 compares FTIR spectra of all samples at room temperature. As shown in Fig. 7, the spectra exhibit a number of absorption bands, mentioning the complex nature of the clay examined. The most distinctive feature of the Mt spectrum is the broad absorption band that ranges from 3400 to 3600 cm^{-1}. The band at 3617 cm^{-1} was associated to the characteristic O–H vibration of smectite. The band at 3426 cm^{-1} was due to O–H stretching of water molecules adsorbed in the interlayer region of the clay. The bending vibrations of water were observed at 1637 cm^{-1}. The band 1044 cm^{-1} was assigned to the stretching vibration of the SiO_4 units, and the bands at 522 and 459 cm^{-1} correspond to bending

vibrations of Al–O–Si and Si–O–Si, respectively. The band at 612 cm^{-1} was assigned to coupled Al–O and Si–O out-of-plane vibrations. The peak intensity observed at about 3426 cm^{-1} was higher than that of the parent clay (Mt) due to the presence of hydroxy-Zr species and hydroxyl groups involved in water–water hydrogen bonds. However, in our case, the peak corresponding to the bending vibration of water molecules at 1637 cm^{-1} was also increased in intensity. The analogy of the FTIR spectra between the Mt and PMt designated that the basic structure of the clay was not altered during the pillaring process.

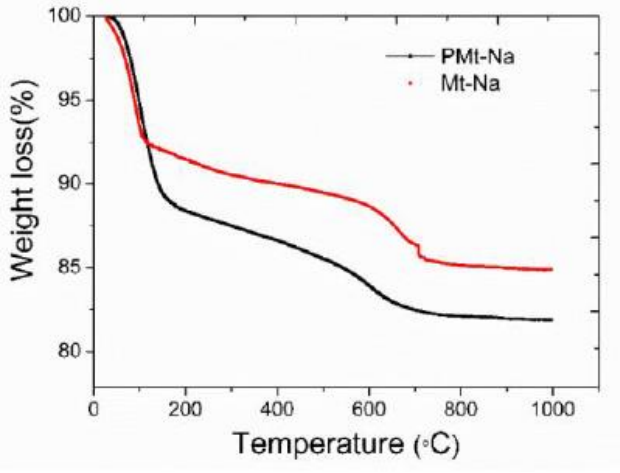

Fig. 6 – FTIR curves of the Mt and PMt.

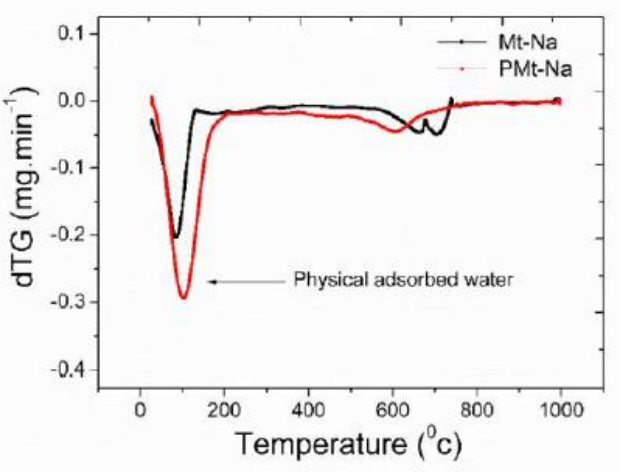

Fig. 7 – Kinetics of BMIMCl intercalation on Mt.

Adsorption of BMIMCl on Mt

The kinetic study aims to determine the time required to reach equilibrium for further experiments. The adsorption kinetics of BMIMCl onto Mt are reported in Fig. 7. The equilibrium is reached after 20 min. The experiment data of adsorption kinetic are fitted by several classical model but the pseudo-second-order kinetic given by Eq. (1) gave the best fit according to the coefficient R^2 up to 0.99 Fig. 8.

$$\frac{dq_t}{dt} = k(q_e - q_t)^2 \qquad (1)$$

where k is the rate constant of the pseudo-second-order model, q_t and q_e are the amounts of solute adsorbed per gram of adsorbent at any time and at equilibrium, respectively. Integration for boundary conditions $t = 0$ to $t = t$ and $q_t = 0$ to $q_t = q_t$ follow by rearrangement gives:

$$q_t = \frac{Kq_e^2.t}{1+Kq_e.t} \qquad (2)$$

The Eq. (2) can be rearranged linear forms as:

$$\frac{t}{q_t} = \frac{1}{kq_e^2} + \frac{1}{q_e}t \qquad (3)$$

Table 2 reports all the kinetic parameters. To go further in our investigation, the isotherm of adsorption was investigated. The adsorption isotherms exhibited similar profiles for all Samples Fig. 9a and Fig. 9b.

The experimental data were fitted with two commonly used models. The Langmuir,[24] model Eq. (4) assumes that the formation of a monolayer onto a homogeneous surface with a finite number site. It also assumes that at the equilibrium, both adsorption and desorption occur.

$$q_e = \frac{K_L q_m C_e}{1+K_L C_e} \qquad (4)$$

where C_e (mg L^{-1}) is the equilibrium concentration of IL in solution, q_e (mg g^{-1}) is the adsorption capacity at equilibrium (mg g^{-1}), the maximum adsorption capacity, and K_L is the effective dissociation constant.

The Freundlich isotherm is an empirical model Eq. (5) usually used for heterogeneous adsorption.[25]

The limitation of this model is that the amount of adsorbed molecule increases indefinitely with the concentration of in the solution.

$$q_e = K_F C_e^{\frac{1}{n}} \qquad (5)$$

where q_e (mg g^{-1}) is the adsorption capacity at equilibrium, C_e (mmol L^{-1}) is the equilibrium concentration in solution, and K_F and n are the physical constants.

According to the R^2, the Langmuir model is the most suitable to describe the experimental data Table 3.

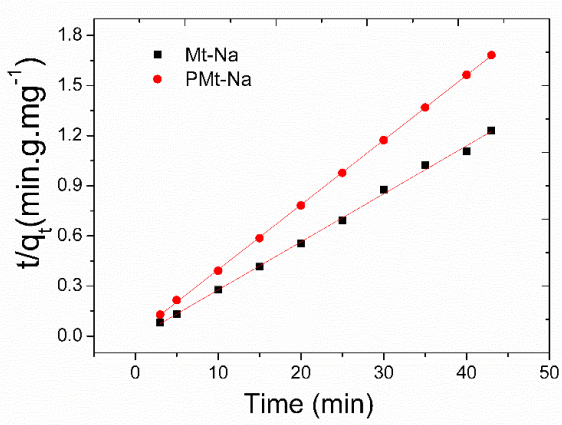

Fig. 8 – Plot *t*/*qt* vs time from the second- order model.

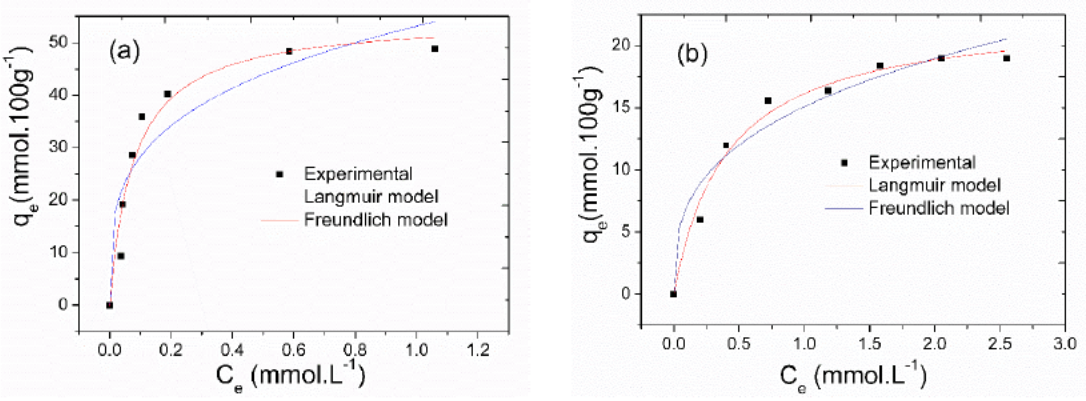

Fig. 9 – BMIMCl sorption isotherms of: a) Mt-Na; b) PMt-Na.

Table 2

kinetic parameters obtained by the Pseudo-second-order model

Pseudo-second-order model			
Sample	q^a_{eq}	K^b	R^2
Mt-Na	34.746	0.073	0.997
PMt-Na	25.773	0.150	0.999

(a) – calculated values [mg·g^{-1}); (b) – calculated values [g·mg^{-1}·min^{-1}].

Table 3

Parameters for the models obtained from Langmuir and Freundlich isotherms

	Langmuir model			Freundlich model		
Sample	q^a_m	k_L	R^2	k_F	n	R^2
Mt-Na	54.77	12.773	0.955	53.112	3.65	0.896
PMt-Na	22.70	2.464	0.986	15.09	3.03	0.950

[a]: calculated values (mmol·100g^{-1})

CONCLUSIONS

Zr-pillared montmorillonite was studied in this work. The microelectrophoresis technique was used for the first time to investigate the electrokinetic surface properties of montmorillonite. The zeta-potential (ζ) analysis of montmorillonite was performed as a function of solution equilibrium pH. The zeta potential of the clay particles was found to be a strong negative surface charge of the montmorillonite, indicating that this clay could be used effectively in the removal of cationic species from the waters. Results obtained from FTIR spectra showed that there were changes in the clay structure with Zr-pillaring. Furthermore, the TGA and DTA methods were used to compare the thermal behavior of the PMt and its corresponding Mt. and demonstrate a two-step process due to the overlapping of clay dehydration processes and silicate structure dihydroxylation.

REFERENCES

1. R. Al-Tohamy, S. S. Ali, F. Li, K. M. Okasha, Y. A. G. Mahmoud, T. Elsamahy, H. Jiao, Y. Fu and J. Sun, *Ecotoxicol. Environ. Safety*, **2022**, *231*, 113160.
2. M. Kashif, M. Yuan, Y. Su, P. M. Heynderickx and A. Memon, *Appl. Clay Sci.*, **2023**, *233*, 106847.
3. C. Breen, *Clay Minerals*, **1992**, *27*, 131–132.
4. F. Figueras, *Catal. Rev. Sci. Eng*., **1988**, *30*, 457–499.
5. S. Yamanaka and G. Brindley, *Clays and Clay Minerals*, **1979**, *27*, 119–124.
6. G. Bartley and R. Burch, *Appl. Catal.*, **1985**, *19*, 175–185.
7. A. Clearfield and P. A. Vaughan, *Acta Crystallographica***, 1956**, *9*, 555–558.
8. E. L. Couch and R. E. Grim, *Clays and Clay Minerals*, **1968**, *16*, 249–256.
9. R. E. Grim and N. Guven, "Bentonites: geology, mineralogy, properties and uses", Elsevier, 2011.
10. A. Belbel, C. Zaouche and N. Djebbari, *Rev. Roum. Chim*., **2023**, *68*, 481–487.
11. X. Yang, G. Shi, C. Wu and H. Sun, *Environ. Sci. Pollution Research*, **2023**, *30*, 24742–24750.
12. A. Serrano-Lotina, R. Portela, P. Baeza, V. Alcolea-Rodriguez, M. Villarroel and P. Ávila, *Catalysis Today*, **2023**, *423*, 113862.
13. M. del Mar Ramos-Tejada, A. Ontiveros, R. del Carmen Plaza, A. V. Delgado and J. D. Durán, *Rheologica Acta*, **2003**, *42*, 148–157.
14. E. Baez, N. Quazi, I. Ivanov and S. N. Bhattacharya, *Advanced Powder Technology*, **2009**, *20*, 267–272.
15. S. García-García, S. Wold and M. Jonsson, *J. Coll. Interface Sci.*, **2007**, *315*, 512–519.
16. J. M. Dzenitis, *Environ. Sci. Technol.*, **1997**, *31*, 1191–1197.
17. A. R. Mermut and G. Lagaly, *Clays and Clay Minerals*, **2001**, *49*, 393–397.
18. H. Van Olphen and J. Fripiar, *Soil Sci.*, **1981**, *131*, 62.
19. A. Haouzi, M. Kharroubi, H. Belarbi, S. Devautour-Vinot, F. Henn and J. Giuntini, *Appl. Clay Sci.*, **2004**, *27*, 67–74.
20. O. Duman and S. Tunç, *Separation Sci. Technol.*, **2008**, *43*, 3755–3776.
21. A. Clearfield, *J. Mater. Research*, **1990**, *5*, 161–162.
22. M. S. Kou, S. Mendioroz and M. Guijarro, *Thermochim. Acta*, **1998**, *323*, 145–157.
23. S. Bodoardo, R. Chiappetta, B. Onida, F. Figueras and E. Garrone, *Microporous and Mesoporous Materials*, **1998**, *20*, 187–196.
24. I. Langmuir, *J. Am. Chem. Soc.*, **1916**, *38*, 2221–2295.
25. Y. Aşçı, M. Nurbaş and Y. S. Açıkel, *J. Hazardous Mater.*, **2008**, *154*, 663–673.